Numerical Analysis of the Cavitating Flow Around a Hydrofoil

Sandor I. BERNAD* Romanian Academy-Timişoara Branch, Romania
sbernad@mh.mec.upt.ro
Romeo SUSAN-RESIGA "Politehnica" University of Timişoara, Romania
resiga@mh.mec.upt.ro
Sebastian MUNTEAN Romanian Academy-Timişoara Branch, Romania
seby@acad-tim.tm.edu.ro
Ioan ANTON "Politehnica" University of Timişoara, Romania
anton@acad-tim.tm.edu.ro

Key words: **cavitation, vapour volume, vapour-liquid interface**

Abstract

Cavitating flows are notoriously complex because they are highly turbulent and unsteady flows involving two species (liquid/vapor) with a large density difference. These features pose a unique challenge to numerical modeling works. This paper reports recent developments and application studies on Computational Fluid Dynamics (CFD) for cavitating flow. The current effort is based on the application of the recently developed full cavitation model that utilizes the modified Rayleigh-Plesset equations for bubble dynamics and includes the effects of turbulent pressure fluctuations to rotating cavitation in different types of fluid turbomachines. Comparisons with available experimental data are used to assess the accuracy of numerical results.

Introduction

In many engineering applications, cavitation has been the subject of extensive theoretical and experimental research since it has predominantly been perceived as an undesirable phenomenon. Cavitation is a rapid phase change phenomenon, which often occurs in the high-speed fluid machineries and it is well known that the cavitating flows raise up the vibration, the noise and the erosion.

The ability to model cavitating flows has drawn strong interest in CFD community. It covers a wide range of applications, such as pumps, turbopumps in rocket propulsion systems, hydraulic turbines, hydrostatic bearings, mechanical heart valve, inducers and fuel cavitation in orifices as commonly encountered in fuel injection systems. Details of the existence, extent and effects of cavitation can be of significant help during the design stages of fluid machinery, in order to minimize cavitation or to account for its effects and optimize the design.

Past several decades have seen considerable research on cavitation and extensive reviews are available in the literature (Ref 1), (Ref 2), (Ref 3). Based on the assumption that the flow is inviscid, various numerical methods have been thus far proposed to simulate cavitating fows; the conformal mapping method, the singularity method, and the panel method. The flow around hydrofoil (Ref 4), (Ref 5), (Ref 6) and within a centrifugal impeller (Ref 7) could be calculated using these inviscid flow models. Experimental observations have revealed that the cavitation appearance relates closely to the viscous phenomena of the liquid-phase, such as the boundary layer and the vortex motion. In the viscous flow models, the Navier-Stokes equation including cavitation bubble is solved in conjunction with Rayleigh's equation governing the change in the bubble radius. Kubota et al. (Ref 5) analyzed the flows around a hydrofoil by the Finite Diference method, and Bunnell et al. (Ref 8) calculated the flow in a fuel injection pump for diesel engines by the control volume method.

To account for the cavitation dynamics in a more flexible manner, recently, a transport equation model has been developed. In this approach volume or mass fraction of liquid (and vapor) phase is convected. Singhal et al. (Ref 9), Merkle et al. (Ref 10) and Kunz et al. (Ref 11) have employed similar models based on this concept with diferences in the source terms. Merkle et al. (Ref 10) and Kunz et al. (Ref 11) have employed the artificial compressibility method. Kunz et al. (Ref 11) have adopted a non-conservative form of the continuity equation and applied the model to diferent geometries. Their solutions are in good agreement with experimental measurements of pressure distributions.

The present work addresses the computational analysis of sheet hydrofoil cavitation. Two-phase cavitating flow models based on homogeneous mixture approach, with a transport equation for the vapor volume fraction have been included in expert commercial codes such as FLUENT (Ref 12). We first evaluate this model for the benchmark problem of a blunt cavitator, and compare the numerical results with experimental data of Rouse & McNown (Ref 13). We have performed such an evaluation for the hemispherical cavitator in (Ref 14). Second, we address the computational analysis of sheet hydrofoil cavitation. The test case corresponds to a NACA 0009 isolated hydrofoil, where experimental data are available in (Ref 15).

Cavitating flow modeling

Numerical simulation of two-phase cavitating flows is an ongoing research effort with the ambitious goal to compute the unsteady evolution for cavities grow and collapse. The CFD community has developed so far a set of mature techniques for simulating single-phase viscous flows, and the past half century of accumulated experience may very well serve to shape the numerical cavitating flow research. This approach is now able to correctly describe partially cavitating two-dimensional hydrofoils, including the re-entrant jet cavity closure model (Ref 16). However, extension to 3D problems and other types of cavitating flows seems to be out of reach for the potential flow model.

Although basic cavitation theoretical studies deal with bubble (or bubble clouds) dynamics by solving for the vapour-liquid interface, most of the practical cavitating flows are approached using a homogeneous flow theory. The main idea is to consider a single variable density fluid, without explicit phase interfaces. This model has emerged after carefully examining available experimental investigations, as well as by evaluating the computational costs involved in cavitating flows modelling.

The mixture model is used in the current work for the numerical simulation of cavitating flows with the FLUENT expert code (Ref 12). In this model, the flow is assumed to be in thermal and dynamic equilibrium at the interface where the flow velocity is assumed to be continuous.

The *mixture* is a hypothetical fluid with variable density,

$$\rho_m = \alpha \rho_v + (1-\alpha)\rho_l \ , \tag{1}$$

ranging from liquid density for $\alpha = 0$ to vapour density ρ_v for $\alpha = 1$. The vapour volume fraction

$$\alpha = \frac{Vol_{vapor}}{Vol_{liquid} + Vol_{vapor}} \ , \tag{2}$$

is an additional unknown of the problem. The mixture will of course satisfy the continuity equation

$$\frac{d\rho_m}{dt} + \rho_m \nabla \cdot u_m = 0 \, , \tag{3}$$

where d / dt denotes the material derivative. Next, one has to consider a momentum equation for the mixture. A simple choice would be to neglect the viscous effects and use the Euler equation. The system of equations can be then closed with a relationship density-pressure (equation of state). However, when considering a barotropic mixture, i.e. the density depends solely on the pressure, some physics is lost. This can be easily seen when writing the vorticity transport equation

$$\frac{\partial \omega}{\partial t} + u \cdot \nabla \omega = \omega \cdot \nabla u + \frac{1}{\rho^2} \nabla \rho \times \nabla p + viscous \ \ terms \ \ . \tag{4}$$

The second term in the right-hand-side, which accounts for the baroclinic vorticity generation, vanishes when $\rho = \rho(p)$. As a results, an important vorticity source is lost, especially in the cavity closure region (Ref 19). Practical computations of industrial flows are using RANS equations with various turbulence modelling capabilities. An alternative to the equation of state is to derive a transport equation for the vapour volume fraction. The continuity Eq. (3), together with Eq. (1), give the velocity divergence as

$$\nabla \cdot u_m = -\frac{1}{\rho_m} \frac{d\rho_m}{dt} = \frac{\rho_l - \rho_v}{\rho_m} \frac{d\alpha}{dt} \ \ . \tag{5}$$

Using Eq. (5), the conservative form of the transport equation for α can be easily written,

$$\frac{\partial \alpha}{\partial t} + \nabla \cdot (\alpha u_m) = \frac{1}{\rho_v}\left[\frac{\rho_v \rho_l}{\rho_m}\frac{d\alpha}{dt}\right] \quad . \tag{6}$$

Eq. (6), can be also written for the liquid volume fraction, $1-\alpha$,

$$\frac{\partial (1-\alpha)}{\partial t} + \nabla \cdot [(1-\alpha) u_m] = \frac{1}{\rho_l}\left[-\frac{\rho_v \rho_l}{\rho_m}\frac{d\alpha}{dt}\right] \quad . \tag{7}$$

The factor in square brackets in the r.h.s. of Eqs. (6) and (7) is the interphase mass flow rate per unit volume:

$$\dot{m} = \frac{\rho_v \rho_l}{\rho_m}\frac{d\alpha}{dt} \quad . \tag{8}$$

If we add term by term Eqs. (6) and (7), we end up with an inhomogeneous continuity equation of the form

$$\nabla \cdot u_m = \dot{m}\left(\frac{1}{\rho_v} - \frac{1}{\rho_l}\right) \quad , \tag{9}$$

which is used in (Ref 3) to replace homogeneous Eq (3).
Finally, the vapour volume fraction transport equation is written as:

$$\frac{\partial \alpha}{\partial t} + \nabla \cdot (\alpha u_m) = \frac{1}{\rho_v}\dot{m} \quad . \tag{10}$$

This is the equation for the additional variable α, to be solved together with the continuity and momentum equations.

Most of the efforts in cavitation modelling are focused on correctly evaluating $\dot{m}$. One approach has been proposed by Merkle et al. (Ref 10), by modelling the phase transition process similar to the chemically reacting flows. This model was successfully employed by Kunz et al. (Ref 11) in a variety of cavitating flows. Senocak and Shyy attempt a derivation of an empiricism-free cavitation model (Ref 17) in order to avoid the evaporation/condensation parameters introduced by Merkle. As a result, the vapour volume fraction can be written as

$$\alpha = \frac{n_b \frac{4}{3}\pi R^3}{1 + n_b \frac{4}{3}\pi R^3} \quad , \tag{11}$$

where the number of bubbles per volume of liquid, n_b, is a parameter of the model.

From (11) we can easily get

$$\frac{d\alpha}{dt} = \alpha (1-\alpha)\frac{3\dot{R}}{R} \quad , \tag{12}$$

where $\dot{R}$ is the bubble vapour-liquid interface velocity. A simplified Rayleigh equation can be used to compute

$$\dot{R} \equiv \frac{dR}{dt} = sgn(p_v - p)\sqrt{\frac{2}{3}\frac{|p_v - p|}{\rho_l}} \quad . \tag{13}$$

Of course the bubble grows if the mixture pressure is less than the vaporization pressure, $p < p_v$, and collapses when $p > p_v$. The bubble collapse, as modelled by the Rayleigh second order differential equation, is much more rapid than the bubble growth. However, the above model seems to make no such difference between grow and collapse.

The present paper employs the mixture model, as implemented in the FLUENT commercial code, with the cavitation model described by Eqs. (8), (12) and (13).

The numerical approach

To simulate the cavitating flow the numerical code FLUENT (Ref 12) was used. The code uses a control-volume-based technique to convert the governing equations in algebraic equations that can be solved numerically. The full Navier-Stokes equations are solved. The flow was assumed to be steady, and isothermal. In these calculations turbulence effects were considered using turbulence models, as the k-ε RNG models, with the modification of the turbulent viscosity for multiphase flow. To model the flow close to the wall, standard wall-function approach was used, then the enhanced wall functions approach has been used to model the near-wall region.

Validation of the cavitating flow model

Before any attempt of computing cavitating hydrofoil flows, we have tested the model described on a benchmark problem. The flow with and without cavitation computed for the axi-symmetric cavitator with blunt fore-body and numerical results are compared with experimental data. For this particular axisymmetric body, Rouse and McNown (Ref 13) have provided the pressure coefficient distribution along the body. In Figure 1, field liquid volume fraction contours and the computational grid are illustrated for the $\sigma = 0.5$ case. The results include steady-state computations of non-cavitating and cavitating flows. From the physical point of view, the steady-state assumption is sensible for sheet cavitation, which has a quasi-steady behavior, with most of the unsteadiness localized in the rear closure region.

Figure 1 shows the distribution of α around a hemispherical fore-body, for a cavitation number

$$\sigma = \frac{p_\infty - p_v}{\frac{1}{2}\rho_l U_\infty^2} = 0.5 \tag{14}$$

Most of the computational domain constrains only liquid, $\alpha = 0$, but within the region with $p < p_v$ the vapour phase is formed with $0 < \alpha < 1$. Cavitation occurs as a result of the flow acceleration over the body surface resulting in regions with pressures lower than the vapor pressure. Then the water transform to vapor in these regions, thereby forming vapor-filled cavities. These cavities collapse when the local pressure becomes larger than vapor pressure, with a reentrant water jet and the flow generally becomes unsteady.

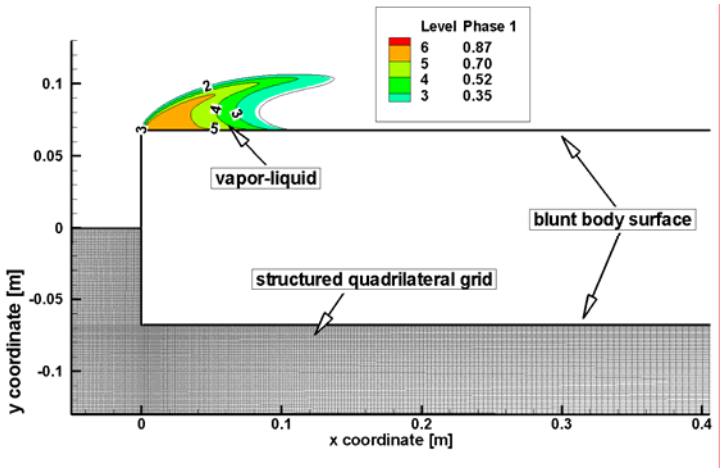

Figure 1. Predicted liquid volume fraction and surface pressure contours, selected streamlines and computational grid for a blunt-body, at cavitation number σ = 0.5.

Thus an irregular cyclic process of bubble formation and growth occurs, followed by the filling and finally breaking off of the bubble. Due to cavitation, large density and viscosity gradients arise at the interfaces between nearly incompressible fluids. The pressure coefficient is plotted against the dimensionless curvilinear abscissa along the body, originating at the axis,

$$c_p = \frac{p - p_\infty}{\frac{1}{2}\rho_l U_\infty^2} \tag{15}$$

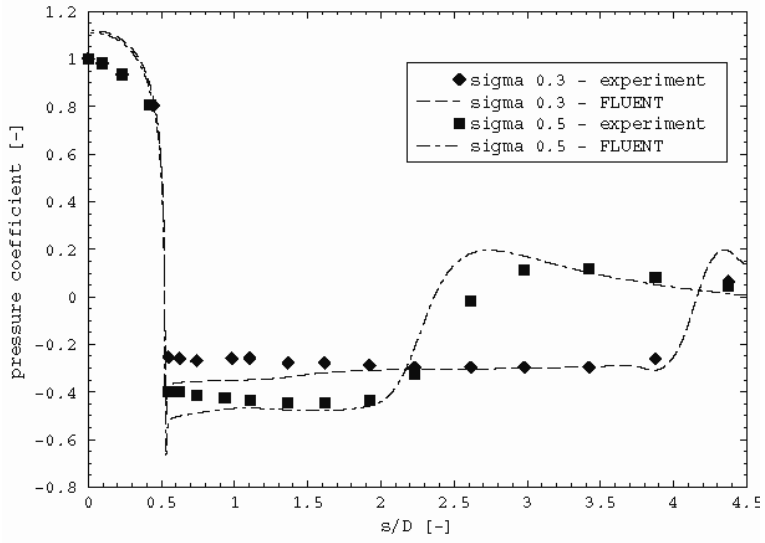

Figure 2. Comparison of predicted and measured surface pressure distributions at several cavitation numbers for a blunt-body.

Figure 2 shows predicted and measured surface pressure distributions at several cavitation numbers for a blunt fore-body with cylindrical afterbody. The model is seen to accurately

capture the bubble size as manifested by the decrease in magnitude and axial lengthening of the suction peak with decreasing cavitation number. Also captured is the overshoot in pressure recovery associated with the local stagnation due to bubble closure. The numerical results correspond to the dashed line, and agree very well with the experimental data (Ref 13). In the cavitation model the vaporization pressure is adjusted to obtain the cavitation number $\sigma = 0.3$ or $\sigma = 0.5$.

Cavitating flow of a NACA 0009 hydrofoil

In this section we examine the fully-wetted flow and the partially cavitating flow for two-dimensional hydrofoils. The main reason for focusing on two-dimensional flow is that particular attention will be given to the method of simulating the flow at the end of the cavity which is a highly turbulent zone characterized by two-phase flow, unsteadiness and instabilities. Thus the rationale is to formulate an accurate model to simulate the two-dimensional flow prior to extending to three dimensions. Most cavity closure models have been formulated to comply with the theoretical analysis of the cavitating flow problem while at the same time attempting to model the physical reality.

We analyze a NACA 0009 hydrofoil at 2.5^0 angle of attack and a cavitation number equal to 0.81, investigated experimentally in (Ref 15). The computational domain is consistent with the experimental setup presented by Dupont (Ref 15). A structured quadrilateral mesh is used for computational domain discretization. Standard boundary conditions for incompressible flow are applied: the velocity is imposed at the inlet (V_{ref}= 20.7 m/s in the present case) and the pressure is fixed at the domain outlet. Then, the pressure is lowered slowly at each new time-step, down to the value corresponding to the desired cavitation number σ defined as $(P_{downstream}-P_{vap})/(\rho_{ref}V_{ref}^2/2)$. Vapor appears during the pressure decrease. The cavitation number is then kept constant throughout the computation. A similar approuch was in (Ref 18).

The presence of a boundary layer will modify the main flow streamlines and subsequently the pressure distribution along the guiding surface. It is important however to distinguish between a cavitation pocket which forms when the liquid detaches itself from the guiding surface, leaving a liquid-free zone, and a separation pocket which forms when the boundary layer separates, leaving a liquid-filled zone. In nearly all cases, the initial point of separation will occur downstream from the point of minimum pressure as the flow up to this point is accelerating. However, cavitation is caused due to the reaching of a particular absolute pressure at any point in the flow. In general, this absolute pressure will be reached at or very close to the guiding surface. Thus at inception, cavitation will occur close to the point of minimum pressure on the surface.

Experiments have revealed that the location of the cavity detachment point can have a significant effect on the cavity extent and the cavity volume. In the case of a sharp leading edge, the cavity will develop from this point. If however, the leading edge is a smooth curve, the cavity detaches from a point downstream of the laminar boundary layer separation point.

The position of the separation and the detachment point and the correlation between them has been studied extensively in literature.

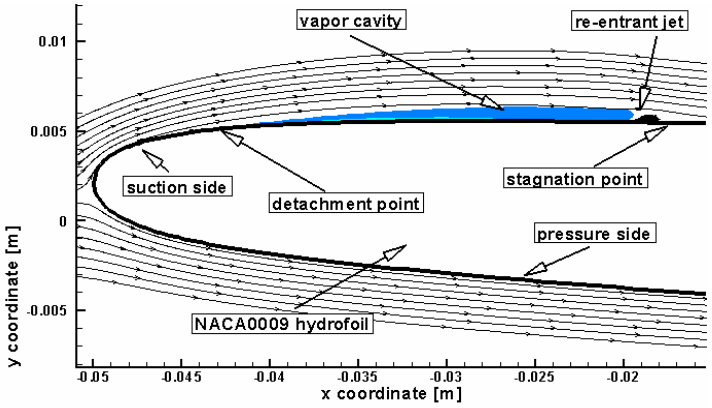

Figure 3. Computed total volume franctions distributions and selected streamlines for NACA 0009 hydrofoil at cavitation number = 0.81.

The gas void fraction contours at the two cavitation numbers are shown in Figure 3. The simulation results indicate the cavity generated on this foil under cavitation number of 0.81 is of stable sheet cavity type. Typical instantaneous pressure contour plots of a cavitating hydrofoil NACA 0009 at non-cavitating and cavitating condition (cavitation number 0.81), are presented in Figures 4 and 5. A region of nearly constant pressure indicating sheet cavity is clearly observable from these figures.

The pressure contours for the flow field at a cavitation number of 0.81 are plotted in Figure 4. We observe that the pressure contours cluster around the cavitation boundary where the density gradient is very large and the flow turns around the cavity. For the cavitation number of 0.81, the cavity extends up to 30 percent of chord. As the cavitation number increases the gas bubble region decreases in length and comes closer to the surface.

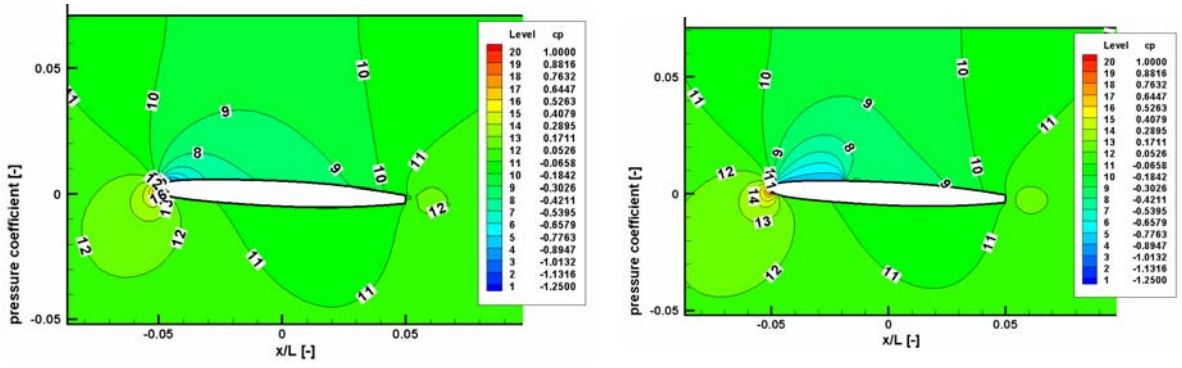

(a) (b)

Figure 4. Pressure coefficient distribution on the NACA 0009 hydrofoil at 2,5 degree angle of attack. a) No cavitation; b) cavitation number 0.81.

Figure 5 shows the comparison of numerical results with experimental data for both non-cavitating and cavitating flows over an isolated NACA 0009 hydrofoil at $2{,}5^0$ angle of attack. An excellent agreement is obtained between simulation and experiment. Moreover, for

cavitating flow we have investigated the effect of turbulence intensity on pressure distribution near the cavity closure. One can see that higher turbulence intensity tends to a sharper cavity closure (dashed line). Although the incoming turbulence intensity is one order of magnitude smaller in the cavitation tunnel, the turbulence intensity levels considered in the present investigation try to account for the flow induced hydrofoil vibrations. The power spectra analysis regarding to the pressure fluctuation corresponding to the higher turbulence intensity near the sharp cavity closure is not investigate in this paper.

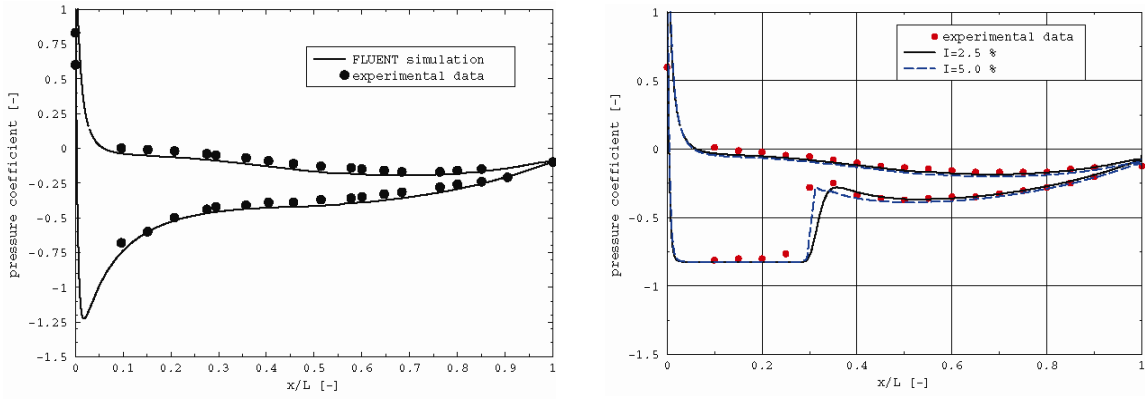

(a) (b)

Figure 5. Pressure coefficient distribution of the different turbulence intensity for NACA 0009 hydrofoil at no-cavitating condition (a) and (b) cavitation number =0.81 .

Conclusions

The paper presents a numerical investigation of cavitating flows using the mixture model implemented in the FLUENT commercial code. The inter-phase mass flow rate is modelled with a simplified Rayleigh equation applied to bubbles uniformly distributed in computing cells, resulting in an expression for the interphase mass transfer. This is the source term for the vapor phase transport equation. As a result, the density of the liquid-vapor mixture is allowed to vary from the vapor density up to the liquid density. The cavitation model is validated for the flow around a blunt fore-body cavitator. The numerical results agree very well both qualitatively and quantitatively with the experiments. As a result we include that the present cavitational model is able to capture the major dynamics of attached cavitating flows.

As the authors proceed with this research, we are focusing on several areas including: 1) improved physical models for mass transfer and turbulence, 2) extended application and validation for steady two-dimensional flows.

Acknowledgments

This work has been supported by Romanian National University Research Council under Grant No. 730/2005. The computation was performed using hardware and software infrastructure on the National Center for Engineering of Systems with Complex Fluids, “Politehnica” University of Timisoara.

References

Ref 1. Arndt, R. E. A., Cavitation in Fluid Machinery and Hydraulic Structures, Ann. Rev. of Fluid Mech., vol. 13, pp. 273-328., 1981.

Ref 2. Li S.C., Cavitation of Hydraulic Machinery, Imperial College Press, 2000.

Ref 3. Kueny, J.L., Cavitation Modeling, Lecture Series: Spacecraft Propulsion, Von Karman Institute for Fluid Dynamics, January 25-29, 1993.

Ref 4. Lohrberg H., Stoffel B., Fortes-Patella R., Coutier-Delgosha O. Reboud JL., Numerical and Experimental Investigations on the Cavitating Flow in a Cascade of Hydrofoils, Experiments in Fluids, 33/4, pp: 578-586, 2002.

Ref 5. Kubota A, Kato H., Yamaguchi H., A new modelling of cavitating flows: a numerical study of unsteady cavitation on a hydrofoil section, J. Fluid Mech., vol. 240, pp. 59-96, 1992.

Ref 6. Shin B.R., Ikohagi T, Numerical analysis of unsteady cavity flows around a hydrofoil, ASME-FEDSM 99-7215, San Francisco, 1999.

Ref 7. Coutier-Delgosha O., Perrin J., Fortes-Patella R., Reboud J.L, A numerical model to predict unsteady cavitating flow behaviour in inducer blade cascades, Fifth int. Symp. On Cavitation, Osaka, Japan, 2003.

Ref 8. Bunnell R.A., Heister S.D., Three-dimensional unsteady simulation of cavitating flows in injector passages, J. Fluid Eng. vol 122, pp 791-797, 2000.

Ref 9. Singhal, A.K., Vaidya, N., Leonard, A.D., Multi-Dimensional Simulation of Cavitating Flows Using a PDF Model for Phase Change, ASME FED Meeting, Paper No. FEDSM'97-3272, Vancouver, Canada, 1997.

Ref 10. Merkle, C.L., Feng, J.Z., and Buelow P.E.O., 1998, Computational modeling of the dynamics of sheet cavitation, Third International Symposium on Cavitation, pp: 307-311, 1998.

Ref 11. Kunz, R.F., Boger, D.A., Chyczewski, T.S., Stinebring, D.R., and Gibeling, H.J., Multi-phase CFD Analysis of Natural and Ventilated Cavitation about Submerged Bodies, Proc. 3rd ASME/JSME Joint Fluid Engineering Conference, Paper FEDSM99-7364, 1999.

Ref 12. FLUENT 6. User's Guide, Fluent Incorporated, 2002.

Ref 13. Rouse, H., and McNown, J.S., Cavitation and Pressure Distribution, Head Forms at Zero Angle of Yaw, Studies in Engineering Bulletin 32, State University of Iowa, 1948.

Ref 14. Susan-Resiga, R.F., Muntean S., Bernad S., Anton, I., Numerical investigation of 3D cavitating flow in Francis turbines, Conference on Modelling Fluid Flow, CMFF'03, Budapest, Hungary, pp: 950-957, 2003.

Ref 15. Dupont P., Etude de la Dynamique d'une Poche de Cavitation Partielle en Vue de la Prediction de l'Erosion dans les Turbomachines Hydrauliques, PhDTthesis, These No. 931, EPFL – Lausanne, 1991.

Ref 16. Krishnaswamy, P., Flow Modelling for Partially Cavitating Hydrofoils, PhD Thesis, Technical University of Denmark, 2000.

Ref 17. Senocak, I., and Shyy, W., Evaluation of cavitation models for Navier-Stokes computations, Proceedings of the 2002 ASME Fluids Engineering Division Summer Meeting, Paper FEDSM2002-31011, 2002.

Ref 18. Ait Bouziad, Y., Physical modelling of leading edge cavitation: Computational methodologies and application to hydraulic machinery, PdD Thesis, Ecole Polytechnique Federale de Lausanne, Suisse, 2005.